Assessment of Plate Theories for Free-Edge Effects

M. d'Ottavio, P. Vidal, E. Valot, O. Polit

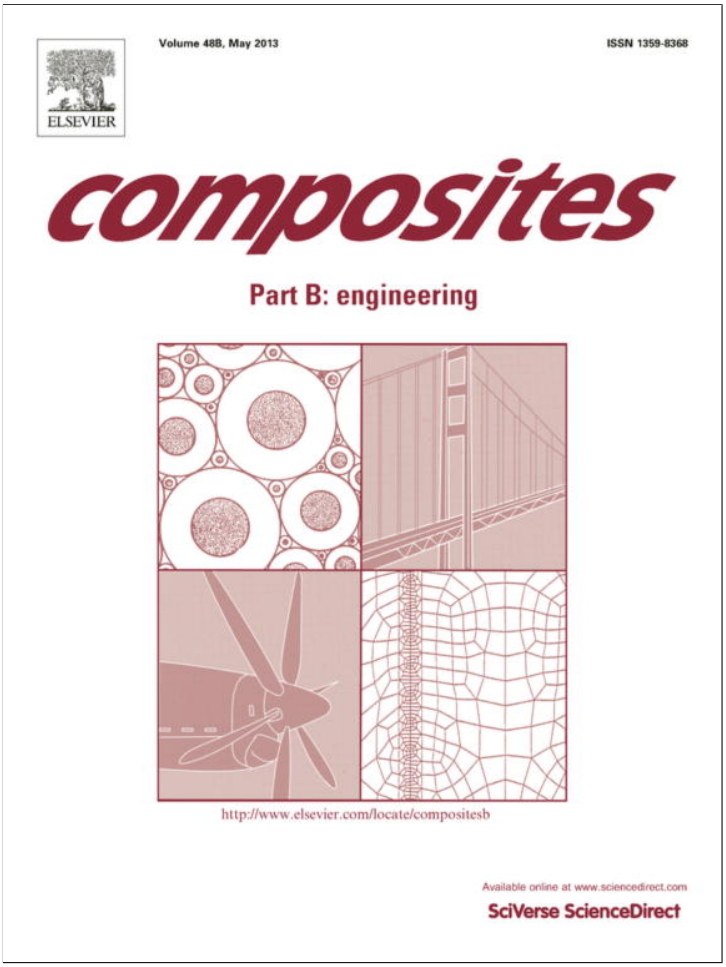

Assessment of plate theories for free-edge effects

Michele D'Ottavio *, Philippe Vidal, Emmanuel Valot, Olivier Polit

LEME – EA4416, Université Paris Ouest, 50, Rue de Sévres, 92410 Ville d'Avray, France

A B S T R A C T

This paper deals with a comparative study of several laminated plate theories with respect to their capability to capture the steep transverse stress gradients occurring in vicinity of free edges. The considered laminated plate theories pertain to the family of Equivalent Single Layer (ESL) as well as Layer-Wise (LW) descriptions. Reference is made to the classical displacement-based approach as well as to a partially mixed variational formulation, which allows to introduce independent assumptions for the transverse stresses and the displacements. Finite element solutions are obtained for free-edge effects that arise in several representative laminates subjected to uniaxial tension. An equivalent stress measure is proposed for assessing the three-dimensional (3D) stress fields predicted by the various theories. It is shown that refined LW models can provide quasi-3D results that compare well with full 3D FEM computations, whereas ESL models fail to capture the free-edge effects. Present results indicate that free-edge effects induced by a ±45° interface are most critical for the accuracy of laminated plate models.

1. Introduction

Fiber-reinforced composites are being increasingly used in weight-sensitive industrial applications, in particular aerospace structures. Composite plate and shell structures basically consist of a stack of several plies whose fiber directions are oriented at different angles. Computational and analytical tools for predicting the behavior of these structures all rely on the so-called effective modulus theory (EMT), in which the heterogeneous fiber–matrix system is homogenized at ply level. As a consequence, elasticity solutions as well as approximated models represent the composite structure as a stack of different homogeneous and anisotropic materials, in which adjacent layers are separated by bi-material interfaces.

Over the last 40 years, much effort has been dedicated to the formulation of appropriate plate/shell models that should cope with the peculiar displacement, strain and stress fields produced by the stiffness distribution across the laminate's cross-section. An overwhelming amount of literature has been produced on this topic, as witnessed by the numerous review articles over composite plate/shell models, e.g., [1–7]. Extensions of models originally formulated for homogeneous structures basically lead to a structural homogenization in which single ply's properties are smeared into an equivalent laminate stiffness. These so-called Equivalent Single Layer (ESL) models have a number of unknown parameters that does not depend on the number of layers constituting the stack. The most widely employed plate models, namely Classical Laminated Plate Theory (CLPT) and First-order Shear Deformation Theory (FSDT), belong to this group [8]. However, these models cannot represent the response at bi-material interfaces where, according to EMT, the transverse stresses need to be continuous (interlaminar equilibrium) and the displacement field has consequently a discontinuous slope along the thickness direction. So-called Zig-Zag models can represent up to a certain extent these interfaces still within an ESL approach [9]. Within EMT, the most refined description considers each ply's properties separately; in these Layer-Wise (LW) models, the number of unknown parameters depends on the number of the represented layers. Three-dimensional (3D) elasticity solutions make evidently use of this layer-wise description.

It is nowadays well established that the simplest 2D models, namely CLPT and FSDT, can be effectively used only for a stiffness design that accounts for the laminate's gross response. If a more accurate representation of the stress field is demanded, for instance for a strength design, refined models should be employed. An assessment permitting clear statements concerning the pertinence of a given model with respect to the investigated response appears thus of major interest. As can be seen in the already cited review articles, most of the papers proposing assessments of 2D plate/shell models refer to rather academic benchmark problems that are essentially limited to the global bending, buckling or free-vibration response and for which exact 3D elasticity solutions may be available as solid reference. However, the main discriminating feature for reduced 2D models is their capability to accurately represent transverse/interlaminar stresses [10]. Configurations with known transverse stress risers appear, hence, as natural candidates for assessing plate models.

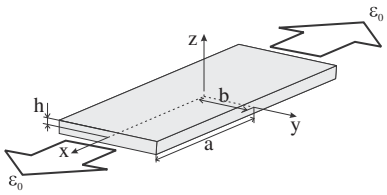

Fig. 1. The Pipes–Pagano problem: composite laminate under uniaxial uniform tensile load.

It is known that relevant transverse stresses arise in presence of in-plane stress gradients and in vicinity of material and/or geometric discontinuities, such as ply-drops, cut-outs and stress-free edges, see, e.g., [11]. Due to its simple implementation within the experimental setup illustrated in Fig. 1, the free-edge effect arising in a composite plate subjected to tensile loads has been extensively studied since the seminal works of Pipes and Pagano [12,13]. Free-edge effects are typical boundary layer effects where a 3D stress concentration is locally confined in a small region in the vicinity of the free edge [14]. While the simple plane stress solution of CLPT holds in the inner region of the plate, no exact elasticity solution is up to now known for the complex 3D stress state at the stress-free edge. Due to the presence of bi-material interfaces, some stress components show even a singular behavior [15–17]. As a consequence, mesh-dependent stress fields are predicted in vicinity of the free edge, which renders questionable the use of these stress components for, e.g., delamination initiation [18]. Dedicated mesh refinement strategies or element formulations have been proposed in the framework of the Finite Element Method (FEM) in order to measure the singularity, see, e.g., [19]. Stress intensity factors can thus be evaluated that may be further used in a delamination onset analysis as in, e.g., [20]. In this context, an attractive alternative to FEM is given by the Boundary Element Method, which appears as an efficient method for the singularity analysis because it permits to substantially reduce the computational effort by confining the dense mesh into the boundary region of concern [21].

Based on the above discussion, the objective of the present paper is to numerically assess a large number of plate models with respect to their capability of representing the stress concentration occurring in the Pipes–Pagano problem illustrated in Fig. 1. The main feature of 2D models is to avoid the cumbersome mesh generation that comes along 3D FEM analysis of general laminate configurations, in which the discretization in the plane (x,y) of the structure depends on that utilized along the laminate's thickness direction z. Most of the assessed models are obtained in the framework of Carrera's Unified Formulation (CUF), which is a compact notation that allows to easily formulate the governing equations for different 2D models [22]. CUF includes ESL and LW models based on either the classical displacement-based approach or the partially mixed approach of Reissner, in which independent assumptions are introduced for the displacement and the transverse stress field [23,24]. It may be interesting to note that the first FEM application of Reissner's partially Mixed Variational Theorem (RMVT) was proposed by Pian and Li and included ESL and LW descriptions for the analysis of stress fields around a hole [25]. Thanks to the systematic procedure of CUF, hierarchic 2D models can be formulated and have been thoroughly assessed in several papers with respect to free-vibration, bending and buckling response of laminated plates and shells, see, e.g., [26–29]. However, an assessment of these models with respect to the free-edge problem, as proposed in the present work, is still missing. In addition to CUF models, the present contribution employs a refinement of the classical sinus model proposed by Touratier [30], which includes transverse normal stress by retaining a quadratic through-the-thickness variation of the transverse displacement as formulated in [31,32].

The outline of this paper is as follows: Section 2 proposes a selective review of several approaches to the Pipes–Pagano problem. CUF models and their FEM implementation are briefly recalled in Section 3 along with the refined sinus model. In Section 4, present numerical results for the Pipes–Pagano problem are first compared with those available in literature. Subsequently, an equivalent stress measure is proposed for the quantitative assessment of the models. The study considers symmetric cross-ply, angle-ply and quasi-isotropic laminates. Furthermore, the paper presents results of 3D FEM computations performed with the commercial software Ansys, against which results from plate models are thoroughly compared. Conclusions are finally summarized in Section 5 along with an outlook towards future investigations.

2. Selected literature review of the Pipes–Pagano problem

An overwhelming amount of literature has been devoted to the classical Pipes–Pagano problem illustrated in Fig. 1. Since an exhaustive review is out of the scope of the present investigation, we refer the interested reader to the more complete surveys of this topic by Mittelstedt and Becker [33,34]. The following selected review is essentially limited to those works whose results are included in the numerical study of the present paper.

In absence of an exact elasticity solution for the free-edge field, approximate solutions have been proposed in semi-analytical closed-form or by means of numerical approximations. The semi-analytical solution approach of Tahani and Nosier [35] solves in closed-form the boundary layer in the direction perpendicular to the stress-free edge (the y direction of Fig. 1), while an approximate solution is found along the through-thickness direction (the z direction of Fig. 1). The latter is defined according to Reddy's layer-wise theory [8] upon discretizing the thickness of each ply in several mathematical layers, in which the field variables are interpolated through linear Lagrange polynomials. Successive refinement can be achieved by increasing the number of mathematical layers in which the plies are divided into (h refinement along the thickness). In this approach, the stress-free conditions at the free edge are thus enforced in an averaged sense by means of weighted integrals. The results of Tahani and Nosier [35] are obtained with 15 subdivisions per ply.

Except the first numerical analysis of the Pipes–Pagano problem provided in [12], which is based on a finite difference scheme, most of the numerical reference solutions have been obtained by means of the Finite Element Method (FEM). Wang and Crossman employed generalized plane strain, three-node triangular elements for discretizing the mid-section $x = 0$ of the laminate [36]. Thanks to the Sky-line storage scheme for the stiffness matrix, Wang and Crossman could use a denser mesh and, hence, provide accurate reference results despite the rather poor computer power available at that time. Subsequent work using the same classical displacement-based FEM focused on the stress singularity at the intersection between the bi-material interface and the free edge [15], and showed that accurate solutions could be found everywhere except in the elements closest to the free edge, i.e., in a region that can be made arbitrarily small upon mesh refinement [37]. The aforementioned works relied on the quasi-3D model (Q3D), which refers to the hypothesis of zero gradients along the axial coordinate x and retaining an axial warping of the (y,z)-planes which depends only on y and z (axis notation according to Fig. 1).

The classical displacement-based method suffers some inherent limitations, in particular the discontinuity of the transverse stress field at the bi-material interface and the approximate satisfaction of the stress-free boundary conditions. So, stress-based equilibrium approaches have been proposed in conjunction with either analytical [38] or numerical FEM-based solutions [39]. Starting

from the mixed Hellinger–Reissner (HR) variational principle, Pagano proposed a sound formulation that permits to express a variationally consistent displacement field starting from only stress assumptions [40]. The mixed HR principle has been employed by Spilker and Chou for developing hybrid-stress FE for the analysis of the Pipes–Pagano problem [41]. Their generalized plane strain quadrilateral has through-thickness cubic and quadratic approximations for the in-plane and transverse displacement, respectively. Independent approximations are introduced for the stress field: σ_{yy}, σ_{zz} and σ_{yz} vary across the thickness of each element with z^3, z^5 and z^4, respectively.

The layer-wise kinematics proposed by Reddy [8], in which the displacement components are interpolated along z through Lagrange polynomials, was successfully applied by Robbins and Reddy to the Pipes–Pagano problem [42]. Eight-node quadratic plate elements have been used to solve the problem in the (x,y)-plane. In addition to the already discussed h refinement along the thickness (i.e., increase of the number of mathematical layers per physical ply), higher-order kinematics have been formulated upon increasing the polynomial order of the interpolation (p-refinement across the thickness); the reported results refer to a model with four mathematical layers and a quadratic polynomial expansion for each layer. The same authors developed in a subsequent work a variable kinematics FEM which permitted to limit the computationally expensive LW plate elements to the free-edge region, while the inner region was modeled by lower-order (FSDT) elements [43].

Based on the classical Q3D modeling assumption, Gaudenzi et al. formulated a 1D FEM in conjunction with several different kinematics for the behavior of the composite cross-section, for which a sublaminate approach was used [44]. By varying the number of sublaminates (or macrolayers) in which the composite section is subdivided, as well as the polynomial order for the through-thickness response inside each sublaminate, this work assessed different models with respect to the Pipes–Pagano problem involving cross-ply and quasi-isotropic laminates. Up to 6th order polynomials were used for the displacement variables in each sublaminate.

As an alternative to LW approximations, Wu and Chen proposed a higher-order ESL displacement model along with a 3-node finite plate element [45]. Fifth and third-order expansions have been used for the in-plane and transverse displacement components, respectively. The exact satisfaction of the interlaminar continuity condition for the transverse shear stress reduces the unknown functions to 18.

In the context of the present paper, it is also interesting to mention other plate models that, in contrast to the works mentioned above, are not classical displacement-based ones. So, the already mentioned mixed approach of Pagano [40] has been employed by Nguyen and Caron for formulating LW finite plate elements dedicated to the analysis of free-edge effects [46]. Furthermore, a partially mixed 2D element has been developed by Desai et al. and successfully applied to the free-edge problem [47].

3. Laminated plate models

The models that are investigated in this work consist in the hierarchic family formulated in Carrera's Unified Formulation (CUF) and in a refined version of the sinus model. The 2D plate equations are numerically solved by FEM. CUF models are all implemented as user elements in the commercial software Abaqus following the formulation proposed by Carrera and Demasi [48]. The plate element based on the refined sinus model has been formulated by Polit et al. [32] and is implemented in the in-house software EvalEF. Since all equations are explicitly reported in various already cited works, in the following only the fundamental relations of the elements shall be briefly summarized along with their main features.

3.1. Description of the composite plate

The cross-section of the laminate of total thickness $2h$ is subdivided in $k = 1, 2, \ldots, N_l$ layers of thickness h_k, see Fig. 2. The through-thickness coordinate $z \in [-h, h]$ can be represented as the sum of N_l layer-specific local coordinates $z_k \in [z_k^b, z_k^t]$, where z_k^b and z_k^t represent the bottom and top interfaces of the kth layer, respectively. The local coordinate is defined by $z_k = z - z_{0k}$, where $z_{0k} = (z_k^t + z_k^b)/2$ identifies the mean surface of the kth layer. A local dimensionless coordinate $\zeta_k \in [-1, 1]$ is introduced for each layer such that $\zeta_k = 2(z_k - z_{0k})/h_k$.

3.2. Hierarchic models in CUF

Plate/shell models may be classified according to their capability to satisfy the bi-material interface conditions, namely the Interlaminar Continuity of transverse stresses (IC) and the associated slope discontinuity (Zig-Zag effect, ZZ) of the displacement field along the composite cross-section. Models based on the Principle of Virtual Displacements (PVD) are formulated upon introducing approximations for the displacement field $u_i = [u_1 \ u_2 \ u_3]^T$. The stress field is then obtained from the compatible strains through the constitutive equation and, therefore, equilibrium at the interfaces may not be satisfied. Reissner's partially mixed variational theorem (RMVT) has been expressly proposed to overcome this drawback by allowing the introduction of independent approximations for the displacements u_i and the transverse stress components $\sigma_{i3} = [\sigma_{13} \ \sigma_{23} \ \sigma_{33}]^T$ [23]. This way, interlaminar stress continuity and slope discontinuity of the displacement field at bi-material interfaces can be *a priori* exactly met, whereas only that part of the constitutive law that involves transverse stresses is satisfied in an integral sense [24]. Moreover, no shear correction factors are required.

The assumptions for the displacement unknowns u_i can be formulated within either an Equivalent Single Layer (ESL) or a Layer-Wise (LW) description. In the ESL case, the through-thickness distribution is defined by polynomials of order N, and the $N+1$ unknown functions $\hat{u}_{is}(x,y)(s = 0, 1, 2 \ldots N)$ are defined for the whole multilayered cross-section:

$$u_i(x,y,z) = \sum_{s=0}^{N} F_s(z)\hat{u}_{is}(x,y) \tag{1}$$

In an LW model, assumptions are introduced for each layer separately as a function of the non-dimensional coordinate ζ_k and by letting explicitly appear the variables at the bottom (b) and top (t) of each layer k:

$$\begin{aligned} u_i^k(x,y,z) &= \sum_{s=0}^{N} F_s(\zeta_k(z))\hat{u}_{is}^k(x,y) \\ &= F_b(\zeta_k)\hat{u}_{ib}^k(x,y) + F_t(\zeta_k)\ \hat{u}_{it}^k(x,y) + \sum_{r=2}^{N} F_r(\zeta_k)\hat{u}_{i\ r}^k(x,y) \end{aligned} \tag{2}$$

The governing equations for the whole laminate are then obtained through an assembly procedure of the N_l layer-specific

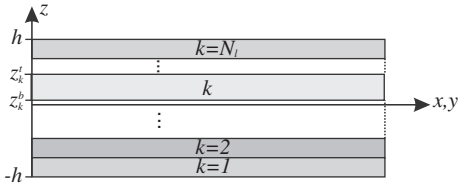

Fig. 2. Coordinate system for the multilayered plate.

contributions. This assembly exactly satisfies the interlaminar continuity conditions $u_i^k(x,y,z_k^t) = u_i^{k+1}(x,y,z_{k+1}^b)$. For RMVT-based models, the assumptions for the transverse stress field σ_{i3} are always introduced within an LW description:

$$\sigma_{i3}^k(x,y,z) = F_b(\zeta_k)\hat{\sigma}_{i3b}^k(x,y) + F_t(\zeta_k)\hat{\sigma}_{i3t}^k(x,y) + \sum_{r=2}^{N} F_r(\zeta_k)\hat{\sigma}_{i3r}^k(x,y) \tag{3}$$

ESL descriptions employ Taylor polynomials, i.e., $F_s(z) = z^s$ in Eq. (1). The slope discontinuity of the displacement field at the interfaces between dissimilar materials can be introduced within an ESL description through the superposition of Murakami's Zig-Zag Function (MZZF) $F_{ZZ}(\zeta_k) = (-1)^k\zeta_k$ and the corresponding ESL unknown function $\hat{u}_{iZZ}$ to the Taylor expansion of Eq. (1) [49]. The interpolation functions $F_s(\zeta_k)$ of the LW description Eq. (2) are constructed from Legendre polynomials and are illustrated in Fig. 3. Note that the linear term ($s = 1$) corresponds to the linear Lagrange interpolation and is only function of the top and bottom variables. In this work, linear ($N = 1$) up to fourth-order ($N = 4$) polynomials are used for all independent variables (i.e., u_i for classical PVD-based models and u_i and σ_{i3} for advanced RMVT-based models).

All CUF models are implemented as isoparametric four-node plate elements based on a bilinear Lagrangian interpolation of all unknown functions, see Fig. 4. For classical PVD-based models, these are $\hat{u}_{is}(x,y)$ for an ESL description and $\hat{u}_{i\ s}^k(x,y)$ for an LW description. For RMVT-based models, the same bilinear approximation is used for the LW transverse stress unknowns $\hat{\sigma}_{i3s}^k(x,y)$. All stiffness contributions are computed exactly through Gaussian quadrature. Note that the (partially) mixed element formulation issued from RMVT may be reduced to a hybrid element by statically condensing out the stress parameters [48]. However, this procedure will not be considered in this paper.

As a result, a large number of 2D elements can be constructed, whose accuracy can be varied upon selection of (i) the underlying variational formulation, (ii) the multilayer description for the displacement field (ESL, ESL + MZZF or LW), and (iii) the polynomial order employed for the assumption. Each model is identified by a unique acronym that is constructed as illustrated in the left part of Fig. 5. The table on the right in Fig. 5 summarizes the capability of the models to *a priori* retain the Interlaminar Continuity of the transverse stress field (IC) and the Zig-Zag behavior of the displacement field at the interfaces (ZZ). Furthermore, the table in Fig. 5 reports the number of degrees of freedom (NDOF) per node that are associated to each element. Some characteristic examples are next given to elucidate the interpretation of the acronyms:

- ED1: PVD-based model with an ESL displacement field that varies linearly over the whole cross-section; NDOF = 6.
- EM2: RMVT-based model with a quadratic ESL displacement field and a quadratic LW transverse stress field; NDOF depends on the number of layers N_l (stress field is LW), e.g., NDOF = 24 if $N_l = 2$ and NDOF = 36 if $N_l = 4$.

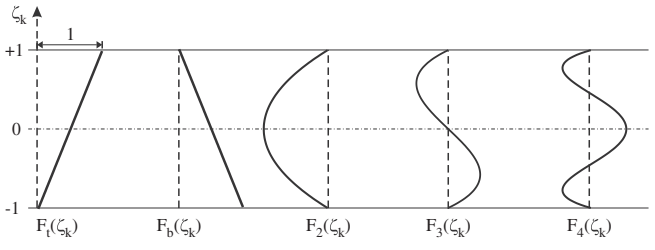

Fig. 3. Through-thickness interpolation functions for LW descriptions.

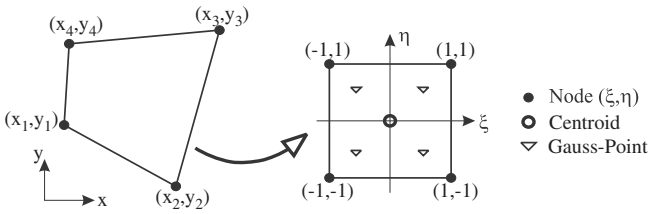

Fig. 4. Isoparametric bilinear FEM interpolation for CUF elements.

- EDZ3: PVD model whose ESL displacement field is obtained by superposing MZZF to a quadratic Taylor expansion; NDOF = 12.
- EMZ2: RMVT model with quadratic transverse stresses in each layer; the ESL displacement assumption is composed of a linear term and of the superposed Zig-Zag function. This FE has the same NDOF as the EM2 element.
- LD4: Most accurate PVD model studied here, in which the displacement field varies according to a fourth-order expansion within each layer. NDOF depends on N_l, e.g., NDOF = 27 for $N_l = 2$ and NDOF = 51 for $N_l = 4$.
- LM4: Most accurate RMVT model studied here, in which displacement and transverse stress fields vary in each layer according to a fourth-order polynomial. NDOF depends on N_l, e.g., NDOF = 54 if $N_l = 2$ and NDOF = 102 if $N_l = 4$.

It is finally worthwhile pointing out following remarks:

1. The number N_l of layers employed for the mathematical description of the laminate may not coincide with the number of plies with dissimilar material which physically constitutes the laminate. Similar to the *h*-refinement, enhanced LW descriptions can be thus obtained upon subdividing each physical ply into several mathematical layers.
2. All CUF models retain the transverse normal deformation and employ the full 3D constitutive law. FSDT is obtained from the linear PVD-based model by penalyzing the transverse normal deformation term and by introducing a shear correction factor (the standard value of $\kappa^2 = 5/6$ will be used). CLPT is obtained from FSDT by additionally penalyzing the transverse shear strain contributions so as to reproduce the Kirchhoff–Love hypotheses. FSDT and CLPT models employ the reduced constitutive law referring to the plane stress condition $\sigma_{33} = 0$.
3. CUF elements are implemented in Abaqus within user subroutines that exploit the parametric definition of CUF models. The selection of the model can be directly made through the standard GUI of Abaqus thanks to dedicated plug-ins written in Python. Visualization of the results is performed through third-party software.

3.3. Refined sinus model

The refined sinus model employed in this work and denoted SZ2, is a PVD-based ESL model that enhances the original sinus model by Touratier [30] upon including the transverse normal stress according to the following kinematics [32]:

$$\begin{cases} U_1(x_1,x_2,x_3=z) = u_0(x_1,x_2) - zu_1(x_1,x_2) \\ \qquad\qquad +f(z)(u_1(x_1,x_2) + \theta_2(x_1,x_2)) \\ U_2(x_1,x_2,x_3=z) = v_0(x_1,x_2) - zv_1(x_1,x_2) \\ \qquad\qquad +f(z)(v_1(x_1,x_2) - \theta_1(x_1,x_2)) \\ U_3(x_1,x_2,x_3=z) = w_0(x_1,x_2) \\ \qquad\qquad +zw_1(x_1,x_2) + z^2w_2(x_1,x_2) \end{cases} \tag{4}$$

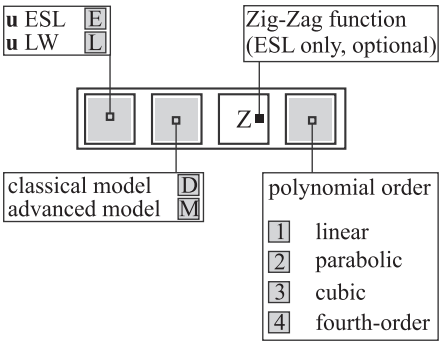

$N = 1 - 4$	ZZ	IC	NDOF
EDN	–	–	$3\,(N+1)$
EDZN	✓	–	$3\,(N+1)$
LDN	✓	–	$3\,(N_l\,N+1)$
EMN	–	✓	$6+3\,N\,(N_l+1)$
EMZN	✓	✓	$6+3\,N\,(N_l+1)$
LMN	✓	✓	$6\,(N_l\,N+1)$

Fig. 5. Hierarchic CUF models: construction of the acronyms (left) and capability of the models to fulfill *a priori* the Zig-Zag behavior (ZZ) and the Interlaminar Continuity of the transverse stresses (IC) (right) along with the associated number of nodal DOF.

Table 1
Material properties of the ply (all moduli and strengths in MPa).

$E_1 = 137{,}900$	$X^+ = 1300$, $X^- = 1000$
$E_2 = E_3 = 14{,}480$	$Y^+ = 70$, $Y^- = 200$
$G_{12} = G_{13} = G_{23} = 5860$	$Z^+ = 100$, $Z^- = 240$
$\nu_{12} = \nu_{13} = \nu_{23} = 0.21$	$Q = 50$, $R = 90$, $S = 70$

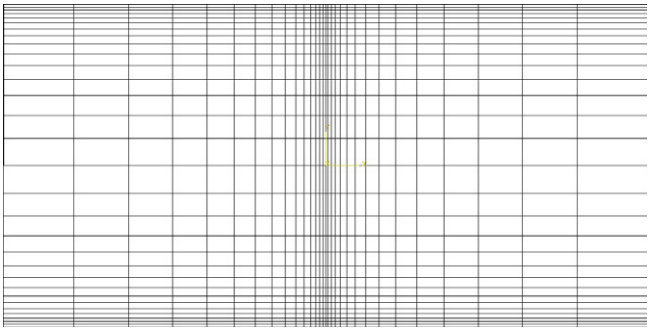

Fig. 6. Mesh employed in the *xy*-plane for the 3D and plate simulations.

where (u_0, v_0, w_0) are the displacements of a point of the middle surface; (v_1, θ_1) and (u_1, θ_2) measure the rotations of the normal transverse fiber about the axis $(0, x_1)$ and $(0, x_2)$, respectively; (w_1, w_2) permit to represent the through-thickness stretch.

As far as the FE interpolation is concerned, an isoparametric approach based on the eight-node quadrilateral finite element is used for (u_0, v_0) and $(u_1, v_1, \theta_1, \theta_2)$. For the set of unknown functions associated with the refinement of the transverse displacement (w_1, w_2), a bilinear finite element approximation is defined using four internal points. These variables can be thus condensed out statically at the element level. A dedicated FE interpolation is used for w_0 for controlling the transverse shear locking according to the "field compatibility" paradigm, see [32] for more details. Therefore, the FE has 7 DOF per node independent of the number of layers (ESL approach).

4. Numerical results

The free-edge effects are investigated by referring to the Pipes–Pagano problem illustrated in Fig. 1. According to the common definition of this classical benchmark, the plate width is taken to be $2b$, the total thickness made of N_l identical plies is $2h = N_l h_k$ and the ratio $b = 4h$ is employed [12,35,36,46]. A uniform axial strain ϵ_0 is applied along the x-axis by prescribing end displacements $\bar{u}$ at $x = \pm a$. All results will be reported in non-dimensional form. The uniform traction load induces a constant strain state along the x-axis in the central region of the plate provided the length a is sufficiently large with respect to the perturbed regions next to the pulled edges. Convergence studies performed with 3D Ansys elements, not shown for the sake of conciseness, have shown that $a = 2b = 8h$ provides a sufficient plate length. All plies are CFRP composites with the material properties given in Table 1. These material properties correspond to those employed in previous reference works [12,35,36,42] and permit, hence, a direct comparison of the results.

In the following, the free-edge effects are studied which arise in classical symmetric laminates, namely the cross-ply laminates $[0°, 90°]_s$ and $[90°, 0°]_s$, the angle-ply laminate $[\pm 45°]_s$ and the quasi-isotropic laminates $[90°, 0°, 45°, -45°]_s$ and $[45°, -45°, 0°, 90°]_s$ [36,44]. In all cases, the symmetry about the mid plane $z = 0$ is exploited to reduce the computational cost.

A mesh with decreasing element size towards the free edge $y = b$ is employed in order to capture the steep gradients of the response. 3D FEM computations with Ansys are performed for providing a reference with solid elements. Appropriate spacing ratios are defined for the 3D mesh which ensure a perfectly cubic shape of the smallest element at the free edge. Several analyses conducted with a different number of elements, not shown for the sake of conciseness, have shown that a mesh with 16×16 elements in the xy-plane is adequate, see Fig. 6. The same mesh is considered in the xy-plane for all 2D plate computations.

At first, the results computed with the most refined CUF elements are validated by comparison against results available in literature as well as Ansys simulations. Subsequently, the different plate models previously described are assessed using a scalar parameter that retains the 3D stress field. Finally, the most accurate approaches are further compared for all the aforementioned laminates.

4.1. Comparison with results available in literature

In this section, the results provided by the quasi-3D approach LM4 using one numerical layer per physical ply are compared with those available in literature. The main features of the involved works have been recalled in Section 2.

The symmetric four-layered laminates $[0°, 90°]_s$ and $[90°, 0°]_s$ are first considered. The only non-zero transverse stress components arising in orthotropic laminates subjected to uniaxial straining along x are due to the Poisson mismatch and are the transverse normal stress σ_{zz} and the transverse shear stress σ_{yz} [34]. Figs. 7 and 8 show their distributions along the y-axis at the bi-material interface and through the thickness at the free edge, respectively. In Fig. 7, LM4 results agree well with the 3D solution for both

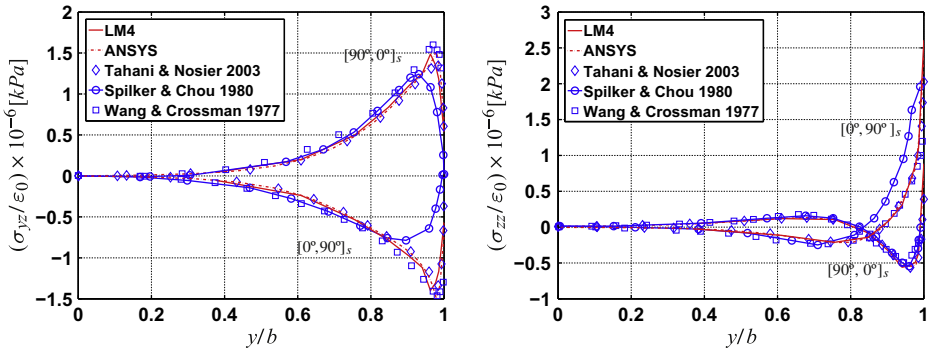

Fig. 7. Interlaminar stresses along y at the bi-material interface $z = h_k$ of cross-ply laminates: σ_{yz} (left) and σ_{zz} (right).

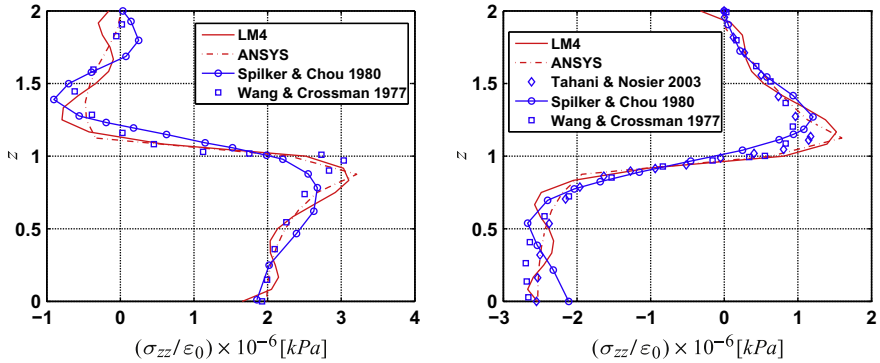

Fig. 8. Through-thickness behavior of σ_{zz} at the free edge ($y = 0.999b$) for cross-ply laminates.

$[0°,90°]_s$ and $[90°,0°]_s$ laminates, in particular the steep rise of the transverse normal stress is well captured. Note that the results of Spilker and Chou [41] show remarkable differences with respect to the behavior near the free edge predicted by Ansys and LM4. Fig. 8 highlights some oscillations of the distribution of $\sigma_{zz}(z)$ obtained by the LM4 model. This may be overcome by adding numerical layers, see Fig. 9. This refinement enhances the representation of the stress-free boundary conditions on the top of the plate as well.

Free-edge stresses in a symmetric angle-ply plate are induced by the extension-shear coupling and concern primarily the transverse shear and normal stress σ_{xz} and σ_{zz}. The distributions of these stress components at the bi-material interface along y and along the thickness at the free edge are given in Figs. 10 and 11, respectively. Again, present LM4 results are very satisfactory as an excellent agreement with the 3D Ansys solution is found. The high gradient at the bi-material interfaces and in the vicinity of the free edge is well estimated, see Fig. 10. Note that the maximum value of the transverse shear stress becomes very high at the free edge. In comparison with the cross-ply laminates, a better agreement is found between present results and those of the literature. We observe that the ESL model of Wu and Cheng [45] is also capable of capturing the steep σ_{xz} gradient at the free edge. A satisfactory agreement is found for the through-thickness distributions $\sigma_{xz}(z)$ and $\sigma_{zz}(z)$ as well, see Fig. 11. As for the results in Fig. 9, increasing the number of numerical layers in each material ply can correct the slightly oscillatory behavior of the LM4 model along with the satisfaction of stress-free conditions at the top face.

Results for the quasi-isotropic laminate $[90°,0°,45°,-45°]_s$ are reported in Fig. 12. The LM4 model is the most suitable to represent the complex behavior of the transverse normal and shear stresses through the thickness at the free edge. In particular, the high stress gradient at the [±45] interface is well-captured.

Once we proved that the most refined CUF model is capable of well capturing the free-edge effects of various laminates, in the next section we shall analyze to what extent less refined 2D models can represent these steep transverse stress gradients.

4.2. Assessment of models

The capability of various CUF models and the SZ2 model to capture the free-edge effect is assessed. A meaningful, though simple, way to compare the accuracy of the stress field predicted by different models consists in defining a representative scalar param-

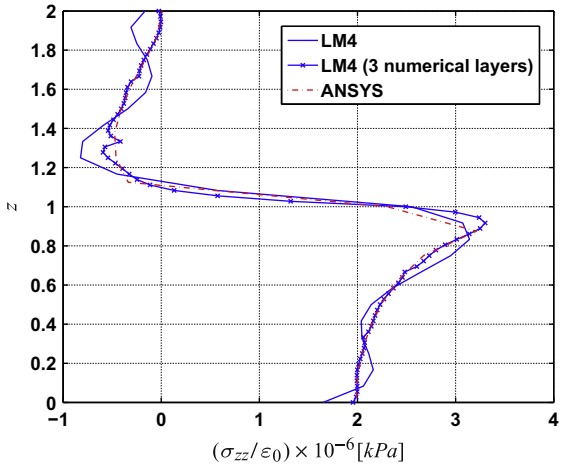

Fig. 9. Through-thickness behavior of σ_{zz} at the free edge ($y = 0.999b$) for the $[0°,90°]_s$ laminate: improvement of LM4 results by using three numerical layers in each ply.

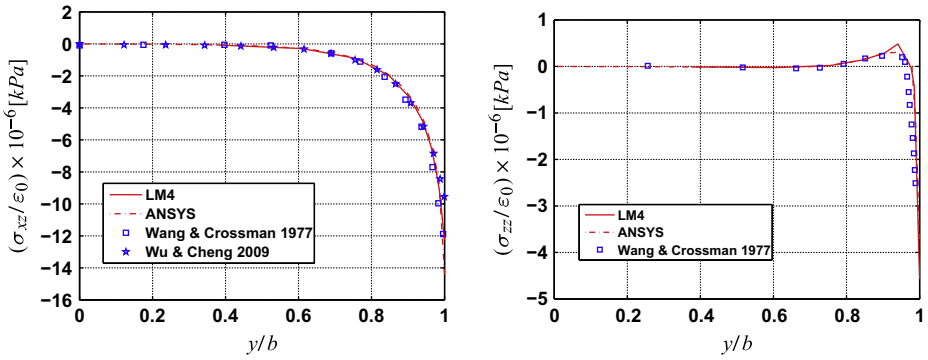

Fig. 10. Distributions along y of the interlaminar stresses σ_{xz} (left) and σ_{zz} (right) at the bi-material interface $z = h_k$ for the angle-ply $[45°, -45°]_s$ laminate.

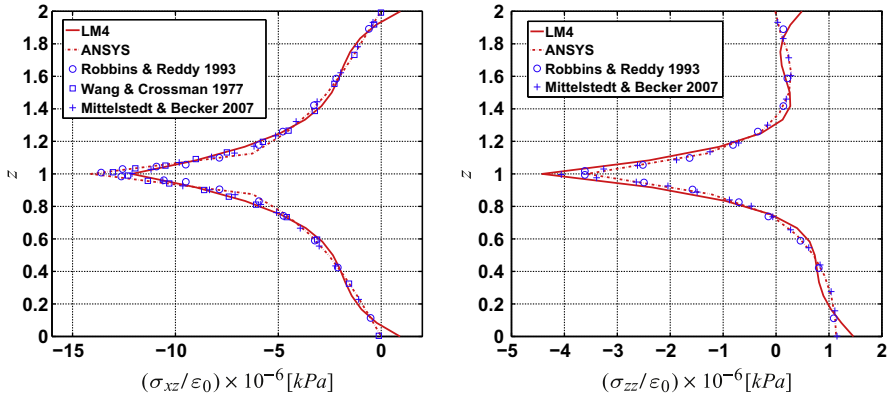

Fig. 11. Through-thickness behavior of σ_{xz} (left) and σ_{zz} (right) at the free edge ($y = 0.999b$) for the angle-ply $[45°, -45°]_s$ laminate.

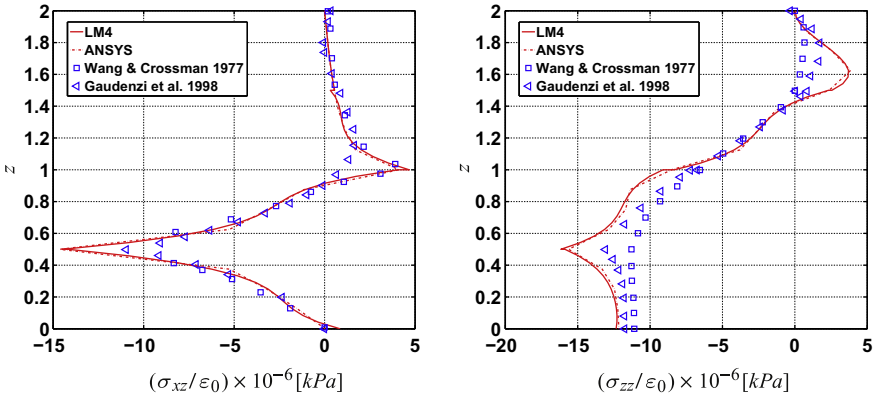

Fig. 12. Through-thickness distributions of σ_{xz} (left) and σ_{zz} (right) at the free edge ($y = 0.999b$) for the quasi-isotropic $[90°, 0°, 45°, -45°]_s$ laminate.

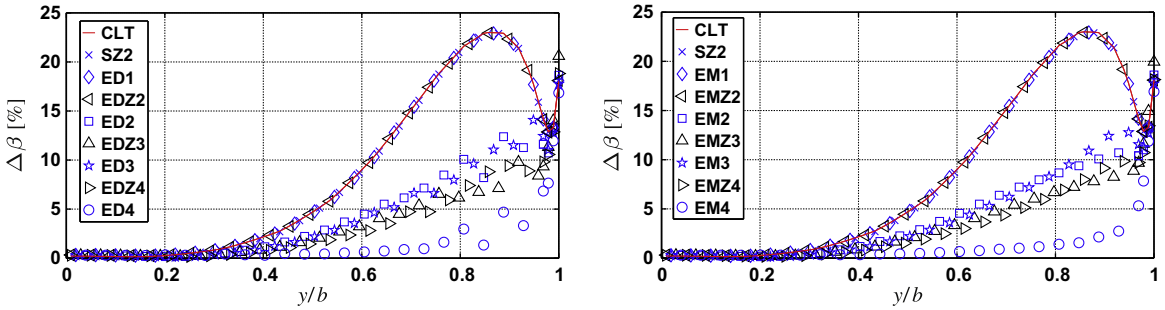

Fig. 13. Error rate $\Delta\beta$ along the y-axis for the quasi-isotropic $[90°, 0°, 45°, -45°]_s$ laminate-ESL models.

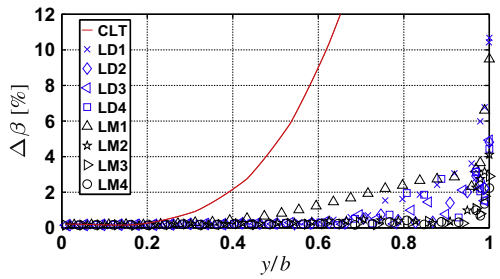

Fig. 14. Error rate $\Delta\beta$ along the y-axis for the quasi-isotropic $[90°,0°,45°,-45°]_s$ laminate-LW models.

eter that encompasses all 6 stress components. This assessment criterion is introduced in Section 4.2.1 and subsequently employed in Section 4.2.2 to classify different model families. The quasi-isotropic laminate $[90°,0°,45°,-45°]_s$ has been taken for this evaluation because it includes different types of bi-material interfaces.

4.2.1. Assessment criterion

A scalar parameter, denoted β, is in the following introduced in order to assess the various plate models. This parameter is constructed by combining all stress components into a single non-dimensional value. Each stress component is herein weighted by its corresponding limit value, that is a material parameter and, hence, independent of the model. The expression for the parameter β reads:

$$\beta = \frac{1}{\sqrt{\alpha}} \quad \text{with } \alpha = \frac{\sigma_{11}^2}{X^2} + \frac{\sigma_{22}^2}{Y^2} + \frac{\sigma_{33}^2}{Z^2} + \frac{\sigma_{23}^2}{Q^2} + \frac{\sigma_{13}^2}{R^2} + \frac{\sigma_{12}^2}{S^2} \tag{5}$$

where X, Y, Z are the normal strengths in the x, y, z directions, and Q, R, S are the shear strengths in the yz, xz, xy planes. The values are given in Table 1, where superscripts + and − denote tensile and compressive strengths, respectively. Despite the similarity of α to classical failure criteria, the parameter β is not meant to be a measure of the criticity of the stress state, i.e., we refrain from referring to any strength consideration concerning the composite material. We remark that the function α describes a convex surface which ensures a finite value for all possible non-nil stress states.

We next define an error rate with respect to the 3D solution based on the parameter β. This error rate is constructed as a weighted average over the whole thickness of the point-wise discrepancies between the values of β issued from the 2D model and the 3D calculation:

$$\Delta\beta[\%] = \frac{\sqrt{\frac{1}{n}\sum_{i=1}^{n}(\beta^{EF} - \beta^{\text{ANSYS}})^2}}{\frac{1}{n}\sum_{i=1}^{n}\beta^{\text{ANSYS}}} \times 100 \tag{6}$$

where n is the number of sampled points through the thickness (a value of $n = 13N_l$ is used throughout this work). Hence, a small value of $\Delta\beta$ indicates that the through-thickness stress distribution obtained from the 2D model recovers well the 3D solution.

4.2.2. Comparison of the CUF and sinus models

In this section, a comparison of the plate models presented in Section 3 is addressed considering the quasi-isotropic laminate $[90°,0°,45°,-45°]_s$. First, the ESL models based on PVD as well as RMVT approaches are assessed. For this purpose, the error rates defined in Eq. (6) are given along the y-coordinate axis in Fig. 13a and b. The curves show that the ED1, EDZ2, SZ2, EM1 and EMZ2 formulations are not suitable for the analysis of free-edge effects. All these models provide results that substantially coincide with CLT ones. A second group of curves can be distinguished, which has an improved accuracy with respect to the previous ones and which comprises the ED2, EDZ3, ED3, EDZ4 models and the corresponding mixed models. The reason for the improved results of these models lies in their refined kinematics that includes the 2nd order term, which allows to retain the transverse stress. Note that the introduction of Murakami's Zig-Zag Function does not bring any significant changes in the value of $\Delta\beta$. We also observe that the odd terms in the z-expansion of the mechanical quantities have no influence, which appears as reasonable due to the simple tensile sollicitation (no bending). Finally, the high-order models ED4 and EM4 drive to the most accurate results.

Fig. 14 reports the error rate $\Delta\beta$ associated to LW models. An improved accuracy of this class of models is evident when compared to the ESL ones of Fig. 13. We observe that the error rate decreases when the order of expansion of the displacement and/or stresses increases. So, the steep gradients of the interlaminar stresses require the use of higher-order approximations in conjunction with LW description. This example shows also that the range of validity of the CLT is limited to the interior of the plate, say $y < 0.5b$.

Neither Fig. 13 nor Fig. 14 show a significant improvement of partially mixed models with respect to displacement-based ones. However, partially mixed models may give more accurate local results, in particular at the interfaces between adjacent plies due to the automatic satisfaction of the interlaminar continuity.

4.3. Comparison of some models for different laminates

For further assessment, the most accurate models identified in Section 4.2 are compared for a wide kind of symmetric laminates, namely cross-ply $[0°,90°]_s$ and $[90°,0°]_s$ (Fig. 15), angle-ply $[\pm45°]_s$ (Fig. 16) and quasi-isotropic $[90°,0°,45°,-45°]_s$, $[45°,-45°,0°,90°]_s$ (Fig. 17). The results obtained from the CLT are also given for comparison.

The comparison between Figs. 15–17 shows that the less severe case is that involving cross-ply laminates, for which even the CLT

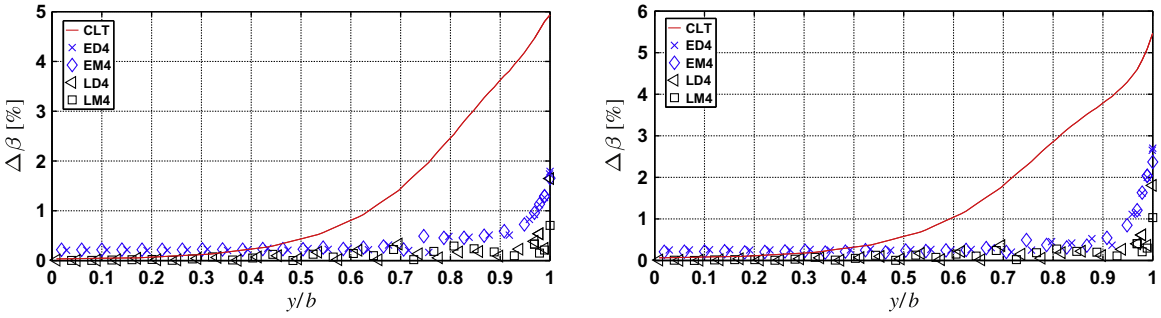

(a) $[90°, 0°]_s$ (b) $[0°, 90°]_s$

Fig. 15. Error rate along the y-axis for the cross-ply laminates.

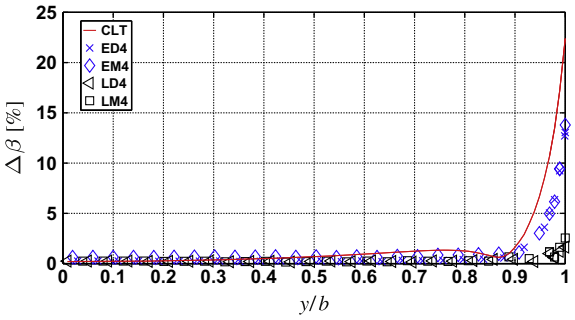

Fig. 16. Error rate along the y-axis for the angle-ply $[45°, -45°]_s$.

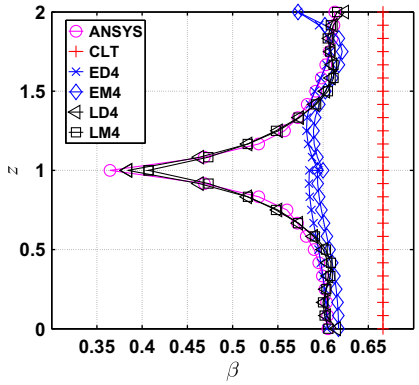

Fig. 19. Through-thickness distribution of the scalar parameter β at the free edge of the angle-ply laminate $[45°, -45°]_s$.

leads to errors less than 6%, whereas the most severe one is that concerning the quasi-isotropic laminate, with errors up to 35%. The angle-ply laminate shows an error rate concentration that is locally confined in vicinity of the free edge. For all configurations, three model groups are again clearly identified, namely CLT, higher-order ESL models and higher-order LW models. The maximum error rate of ED4 and EM4 is about 3% for the cross-ply, about 15% for the angle-ply and about 20% for the quasi-isotropic laminates. For the same lamination schemes, the maximum error rates of LW models are of the order of 2%, 2.5% and 5%, respectively. Finally, the difference between PVD and RMVT models is only marginal, with a slightly superior performance of the partially mixed models.

In order to gain further insight concerning the performance of these higher-order ESL and LW models, the through-thickness distribution of the scalar parameter β at the free edge is shown in Figs. 18–20 for the cross-ply, angle-ply and quasi-isotropic laminates, respectively. The 3D solution from Ansys is given as a reference together with that provided by the CLT. For the cross-ply laminates (Fig. 18), the parameter is nearly constant within each layer, with a higher value in the 0° ply. The results are rather close for the considered CUF models, with ESL models driving to small discrepancies that are limited to the 0° ply. For the three other stacking sequences, Figs. 19 and 20 show that the main error source for ESL models is the steep gradient occurring at the ±45° interface. On the contrary, the LW approach gives accurate results in excellent agreement with the reference 3D solution, even in the most complex case involving quasi-isotropic laminates.

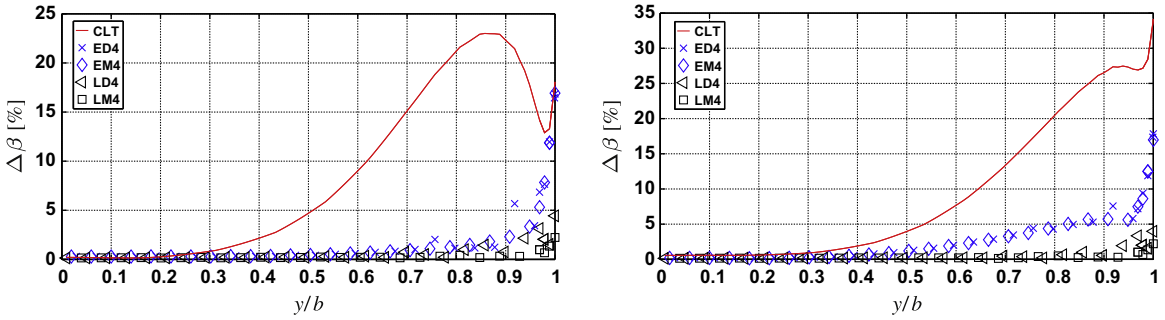

(a) $[90°, 0°, 45°, -45°]_s$ (b) $[45°, -45°, 0°, 90°]_s$

Fig. 17. Error rate along the y-axis for the quasi-isotropic laminates.

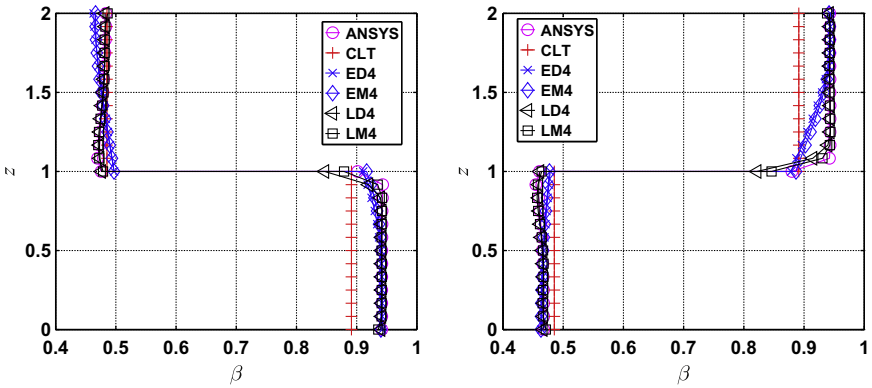

(a) $[90°, 0°]_s$ (b) $[0°, 90°]_s$

Fig. 18. Through-thickness distribution of the scalar parameter β at the free edge of cross-ply laminates.

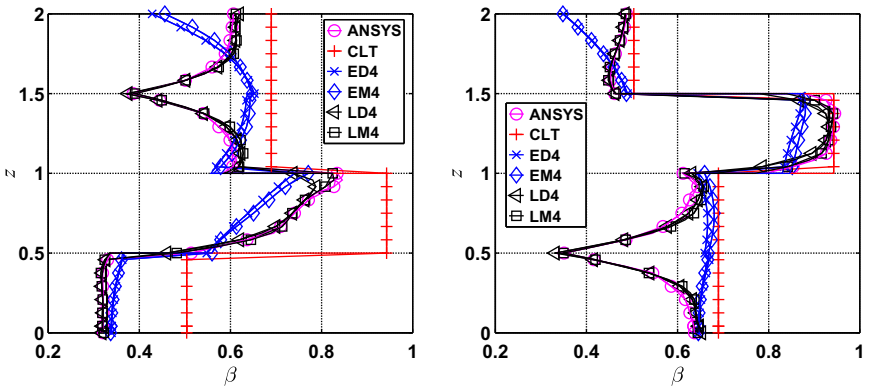

(a) $[45°, -45°, 0°, 90°]_s$ (b) $[90°, 0°, 45°, -45°]_s$

Fig. 20. Through-thickness distribution of the scalar parameter β at the free edge of quasi-isotropic laminates.

5. Conclusions and outlook

Various plate models have been assessed with respect to the free-edge effect of the Pipes–Pagano problem. ESL and LW as well as displacement-based and partially mixed models issued from Carrera's Unified Formulation (CUF) and a refined sinus model have been compared against results available in literature and against 3D solutions obtained from 3D Ansys simulations. After a first comparison of the transverse stress fields occurring in cross-ply, angle-ply and quasi-isotropic laminates, the assessment has been performed on the basis of a representative scalar parameter that encompasses all six stress components. The results have shown that the most critical configuration is that occurring in quasi-isotropic laminates and that the plate models have most difficulties in capturing the steep stress gradients arising at the ±45° interfaces. The relevance of the quadratic term in the z-expansion of the kinematics has been highlighted, which permits to retain the transverse normal stress. High-order LW models recover with very good accuracy the reference 3D solution, whereas high-order ESL models fail to grasp the steep gradients at bi-material interfaces. These results show that refined LW plate models can provide accurate 3D stress states without the need of the cumbersome 3D mesh generation associated with 3D FEM analysis.

The following points can be devised as future perspectives. Due to the rapid decay of the free-edge effects, a fully 2D global–local modeling approach as proposed in [43], in which high-order LW models are confined in vicinity of the free edge, appears as a viable modeling strategy that offers a good accuracy at a moderate computational cost. Since CUF employs the same thickness expansion for all variables, a more rational distribution of the computational effort can be achieved by selecting different approximations for the field variables, as accomplished by the Generalized Unified Formulation of Demasi [50]. The analysis of different configurations, such as free-edge effects in plate bending or around a hole, can provide further insight on the performances of plate models.

Interlaminar stress analysis can be finally completed by a delamination initiation investigation. Here, great attention should be given to the stress singularity at the free edge, which calls for the use of an energy criterion [51]. As recently demonstrated for the layerwise stress approach of [46], a converged evaluation of the stress intensity factors can be achieved within a 2D FEM mesh with a sufficiently refined ply subdivision, in particular in proximity of the bi-material interfaces [52]. A consequent experimental correlation is here necessary.

References

[1] Kapania RK. A review on the analysis of laminated shells. J Pressure Vessel Tech 1989;111:89–96.
[2] Noor AK, Burton WS. Assessment of shear deformation theories for multilayered composite plates. Appl Mech Rev 1989;42:1–13.
[3] Noor AK, Burton WS. Assessment of computational models for multilayered composite shells. Appl Mech Rev 1990;43:67–97.
[4] Reddy JN, Robbins Jr DH. Theories and computational models for composite laminates. Appl Mech Rev 1994;47:147–69.
[5] Carrera E. Theories and finite elements for multilayered, anisotropic, composite plates and shells. Arch Comput Methods Eng 2002;9:87–140.
[6] Rohwer K, Friedrichs S, Wehmeyer C. Analyzing laminated structures from fibre-reinforced composite material-an assessment. Techn Mechanik 2005;25:59–79.
[7] Zhang YX, Yang CH. Recent developments in finite element analysis for laminated composite plates. Compos Struct 2009;88:147–57.
[8] Reddy JN. Mechanics of Laminated Composite Plates and Shells: Theory and Analysis. second ed. CRC Press; 2004.
[9] Carrera E. Historical review of zig-zag theories for multilayered plates and shells. Appl Mech Rev 2003;56:287–308.
[10] Kant T, Swaminathan K. Estimation of transverse/interlaminar stresses in laminated composites-a selective review and survey of current developments. Compos Struct 2000;49:65–75.
[11] Saeger KJ, Lagace PA, Shim DJ. Interlaminar stresses due to in-plane gradient stress fields. J Compos Mater 2002;36:211–27.
[12] Pipes RB, Pagano NJ. Interlaminar stresses in composite laminates under uniform axial extension. J Compos Mater 1970;4:538–48.
[13] Pagano NJ, Pipes RB. The influence of stacking sequence on laminate strength. J Compos Mater 1971;5:50–7.
[14] Allix O, Dupleix-Couderc C. A plate theory as a mean to compute precise 3D solutions including edge effects and related issues. In: Pimenta PM et al., editors. New Trends in Thin Structures: Formulation. Optimization and Coupled Problems, CISM Courses and Lectures, vol. 519. Springer Vienna; 2010. p. 1–28.
[15] Raju IS, Crews Jr JH. Interlaminar stress singularities at a straight free edge in composite laminates. Comput Struct 1981;14:21–8.
[16] Wang SS, Choi I. Boundary-layer effects in composite laminates – Part 1: Free-edge stress singularities. J Appl Mech 1982;49:541–8.
[17] Bar-Yoseph P, Avrashi J. On the nature of the free edge stress singularity in composite laminated plates. Int J Numer Methods Eng 1988;26:1507–23.
[18] Whitney JM, Nuismer RJ. Stress fracture criteria for laminated composites containing stress concentrations. J Compos Mater 1974;8:253–65.
[19] Gu L, Belytschko T. A numerical study of stress singularities in a two-material wedge. Int J Solids Struct 1994;31:865–89.
[20] Leguillon D. A method based on singularity theory to predict edge delamination of laminates. Int J Fract 1999;100:105–20.
[21] Davì G, Milazzo A. Boundary element solution for free edge stresses in composite laminates. J Appl Mech 1997;64:877–84.
[22] Carrera E. Theories and finite elements for multilayered plates and shells: a unified compact formulation with numerical assessment and benchmarking. Arch Comput Methods Eng 2003;10:215–96.
[23] Reissner E. On a certain mixed variational theorem and a proposed application. Int J Numer Methods Eng 1984;20:1366–8.
[24] Carrera E. Developments, ideas and evaluations based upon Reissner's mixed variational theorem in the modeling of multilayered plates and shells. Appl Mech Rev 2001;54:301–29.
[25] Pian THH, Li MS. Stress analysis of laminated composites by hybrid finite elements. In: Kuhn G, Mang H, editors. Discretization Methods in Structural

Mechanics: IUTAM/IACM Symposium Vienna, Austria, 1989. Springer-Verlag. p. 363–72.
[26] Carrera E. Single- vs. multilayer plate modelings on the basis of Reissner's mixed theorem. AIAA J 2000;38:342–52.
[27] Carrera E. A priori vs. a posteriori evaluation of transverse stresses in multilayered orthotropic plates. Compos Struct 2000;48:245–60.
[28] Ciuffreda A, Carrera E. A unified formulation to assess theories of multilayered plates for various bending problems. Compos Struct 2005;69:271–93.
[29] D'Ottavio M, Carrera E. Variable-kinematics approach for linearized buckling analysis of laminated plates and shells. AIAA J 2010;48:1987–96.
[30] Touratier M. An efficient standard plate theory. Int J Eng Sci 1991;29:901–16.
[31] Vidal P, Polit O. A refined sine-based finite element with transverse normal deformation for the analysis of laminated beams under thermomechanical loads. J Mech Mater Struct 2009;4:1127–55.
[32] Polit O, Vidal P, D'Ottavio M. Robust C^0 high-order plate finite element for thin to very thick structures: mechanical and thermo-mechanical analysis. Int J Numer Methods Eng 2012;90:429–51.
[33] Mittelstedt C, Becker W. Interlaminar stress concentrations in layered structures: Part I – A selective literature survey on the free-edge effect since 1967. J Compos Mater 2004;38:1037–62.
[34] Mittelstedt C, Becker W. Free-edge effects in composite laminates. Appl Mech Rev 2007;60:217–45.
[35] Tahani M, Nosier A. Free edge stress analysis of general cross-ply composite laminates under extension and thermal loading. Compos Struct 2003;60:91–103.
[36] Wang ASD, Crossman FW. Some new results on edge effect in symmetric composite laminates. J Compos Mater 1977;11:92–106.
[37] Whitcomb JD, Raju IS, Goree JG. Reliability of the finite element method for calculating free edge stresses in composite laminates. Compos Struct 1982;15:23–37.
[38] Kassapoglou C, Lagace PA. An efficient method for the calculation of interlaminar stresses in composite materials. J Appl Mech 1986;53:744–50.
[39] Rybicki EF. Approximate three-dimensional solutions for symmetric laminates under inplane loading. J Compos Mater 1971;5:354–60.
[40] Pagano NJ. Stress fields in composite laminates. Int J Solids Struct 1978;14:385–400.
[41] Spilker RL, Chou SC. Edge effects in symmetric composite laminates: importance of satisfying the traction-free-edge condition. J Compos Mater 1980;14:2–20.
[42] Robbins Jr DH, Reddy JN. Modelling of thick composites using a layerwise laminate theory. Int J Numer Methods Eng 1993;36:655–77.
[43] Robbins Jr DH, Reddy JN. Variable kinematic modeling of laminated composite plates. Int J Numer Methods Eng 1996;39:2283–317.
[44] Gaudenzi P, Mannini A, Carbonaro R. Multi-layer higher-order finite elements for the analysis of free-edge stresses in composite laminates. Int J Numer Methods Eng 1998;41:851–73.
[45] Zhen Wu, Chen Wanji. A higher-order displacement model for stress concentration problems in general lamination configurations. Mater Des 2009;30:1458–67.
[46] Nguyen VT, Caron JF. A new finite element for free edge effect analysis in laminated composites. Comput Struct 2006;84:1538–46.
[47] Ramtekkar GS, Desai YM. On free-edge effect and onset of delamination in FRPC laminates using mixed finite element model. J Reinf Plast Compos 2009;28:317–41.
[48] Carrera E, Demasi L. Classical and advanced multilayered plate elements based upon PVD and RMVT. Part 1: Derivation of finite element matrices. Part 2: Numerical implementations. Int J Numer Methods Eng 2002;55:191–231. 253–291.
[49] Murakami H. Laminated composite plate theory with improved in-plane response. J Appl Mech 1986;53:661–6.
[50] Demasi L. Invariant finite element model for composite structures: the generalized unified formulation. AIAA J 2010;48:1602–19.
[51] Martin E, Leguillon D, Carrère N. A twofold strength and toughness criterion for the onset of free-edge shear delamination in angle-ply laminates. Int J Solids Struct 2010;47:1297–305.
[52] Saeedi N, Sab K, Caron JF. Delaminated multilayered plates under uniaxial extension. Part II: Efficient layerwise mesh strategy for the prediction of delamination onset. Int J Solids Struct 2012;49:3727–40.